Magnetic disaccommodation phenomena in rare-earth intermetallic compounds

L. M. García, J. Bartolomé, and F. J. Lázaro
Instituto de Ciencia de Materiales de Aragón, Consejo Superior de Investigaciones Cientificas-Universidad de Zaragoza, 50009 Zaragoza, Spain

C. de Francisco and J. M. Muñoz
Departamento de Electricidad y Electrónica, Universidad de Valladolid, Valladolid, Spain
(Received 14 March 1996; revised manuscript received 11 July 1996)

On the $R_2Fe_{14}B$ (R=rare earth) pure and hydrogenated compounds a systematic ac magnetic susceptibility study has been performed, to determine the origin of a frequently observed anomaly, nonrelated to the spin reorientation transitions. We have been able to induce the anomaly by thermal annealing the ingots, and to increase its height increasing both the annealing time and temperature. This susceptibility anomaly has been correlated with a similar one found, for the same samples, at the same temperature in magnetic aftereffect (MAE) measurements. We conclude that the anomaly is caused by magnetic disaccommodation of point defects coupled to the domain walls. Based on this mechanism a simple model is proposed, which interprets the phenomenology of this type of anomalies. For all samples measured and with activation energy and relaxation time parameters for the domain wall motion (coupled to defects) obtained from MAE experiments, the real and imaginary components of the susceptibility data have been fitted to the appropriate analytical expressions. [S0163-1829(96)09645-2]

I. INTRODUCTION

The measurement of the ac initial magnetic susceptibility, χ_{ac}, is a technique widely used in the study of physical properties of magnetic materials, due to its high sensitivity to detect magnetic phase transitions.[1] The renewed interest in rare earth (R) transition metal (T) intermetallic compounds for permanent magnet applications[2–4] has enhanced the study of the anomalies associated with their magnetic spin reorientation phase transitions (SRT) and, therefore, a large amount of χ_{ac} data have been produced. Due to the very nature of χ_{ac}, which is sensitive both to the intrinsic and extrinsic properties of the samples, it strongly depends on microstructure, impurities, defects, etc. of the samples and some anomalies (non-SRT) in χ_{ac} may be due to other causes besides a spin reorientation transition. In this context, we stress that most of the measurements have been performed on polycrystalline samples and their anomalies are smeared out.[5]

In many intermetallic compounds the non-SRT anomaly has often been found at thermal range 150 to 250 K and in all cases the anomaly shows similar magnetic and thermodynamic behavior. Its origin has been the subject of a number of conjectures and conflicting interpretations and we aim to shed some light on the origin of this anomaly. To this aim we feel it is worth to briefly review the existing data and interpretations on the most relevant series of rare earth transition metal intermetallic compounds.

On $R_2T_{14}Z$ compounds (R=Nd, Sm, Tb, Dy, Ho, Er, Tm; T=Fe, Co; Z=B, C)[6] the non-SRT anomaly has always been detected at the same thermal range (200 to 260 K). For $Nd_2T_{14}B$ and $Pr_2T_{14}B$ the anomaly was assumed to be correlated with the critical temperature at which first order magnetization process (FOMP) transitions appeared.[7] Unluckily, the interpretation is in conflict with the counterexamples R=Sm, Tb, Dy, Er, Tm where the anomaly is present, but no FOMP's are known to exist. $Sm_2Co_{14}B$ has the same kind of anomaly and it was explained as due to a SRT in the basal plane.[8] However, this transition has never been corroborated by magnetization measurements.

The anomaly has also been detected in a $Nd_2Fe_{14}B$ single crystal, when $\chi_{ac}(T)$ was measured along the c direction (tetragonal symmetry).[9] This is an important result since it allows to disregard some of the proposed origins for the anomaly, namely magnetic ordering of spurious phases[10] or superparamagnetic blocking of small particles.[11] However important it is, other single crystals of the same or different composition have shown no anomalies.[12,13]

Besides the pure compounds, the non-SRT anomaly has also been detected in hydrogenated materials, particularly in $Ho_2Fe_{14}BH_x$,[14] and it was reported that the anomaly shifted to lower temperatures as hydrogen amount increased. The existence of the anomaly was ascribed to the onset of a collinear to noncollinear magnetic phase transition. For $Pr_2Fe_{14}BH_x$ the origin of the anomaly was correlated with a SRT induced by hydrogen uptake.[15]

The R_2Fe_{17} compounds provide further phenomenology. Sm_2Fe_{17}, which has no SRT in the whole thermal range,[16,17] shows a clear anomaly around 165 K.[18,19] This anomaly was interpreted as due to a strong variation of the anisotropy, caused by the higher than second order crystal electric field terms of the Sm^{3+} ion.[19] Moreover, the anomaly shifts to higher temperatures if there is interstitial carbon, while the insertion of interstitial nitrogen induces a new anomaly.[20] It was conjectured that the anomaly was caused by a SRT or FOMP, but these transitions were not observed up to a field of 35 T and the conjecture was dropped.[21]

Kronmüller *et al.*[22] showed that an anomaly appears in magnetic aftereffect (MAE) measurements on Sm_2Fe_{17} and two anomalies in its nitride $Sm_2Fe_{17}N_x$, at the thermal range 200 to 250 K. The MAE anomaly was assigned to thermally

activated jumps of iron vacancies and interstitial nitrogen atoms. For $Nd_2Fe_{14}B$ (Ref. 23) and $R_2Fe_{14}BH_x$,[24] we also confirmed the existence of correlation between the anomalies detected which appear in $\chi_{ac}(T)$ and MAE measurements. For $Sm_2Fe_{17}H_x$ this correlation has recently been reported.[25,26]

For R_2Co_{17} (R=Tb, Dy, Ho) again the non-SRT anomaly has been found at the thermal range 150–200 K.[27] It was interpreted as due to the combination of two opposed effects: domain wall motion (DWM), which increases as temperature rises,[9] vs planar anisotropy, which decreases with increasing temperature, and might become very small.

Once again, the same non-SRT anomalies have been detected for $RFe_{11}Ti$ (R=Nd, Sm, Er, Tm) at the thermal range 200 to 250 K (Ref. 28) and explained as above. Moreover, for $RFe_{11}Mo$ (R=Ho, Er, Tm, Lu, Y, Sm) similar anomalies as in the Ti-based compounds have been measured. For the Sm compound the anomaly was assigned to the existence of a FOMP, while in the other compounds it was correlated with an unknown phase transition of the Fe sublattice.[29] The study was extended to the Y and Lu (nonmagnetic elements) compounds and their anomalies in $\chi_{ac}(T)$ were ascribed to spin-glass-like magnetic transitions, because of their magnetic relaxation behavior.[30] Moreover, for R=Er, Tm, and Ho the origin of the anomaly was assigned to a spin-glass-like behavior, due to frustrated magnetic ordering in the Fe-Mo sublattices.[31] However, recent $\chi_{ac}(T)$ measurements performed on these Mo-based compounds have not detected these anomalies.[32]

Finally, analogous anomalies have been reported on the recently discovered family $R_3(Fe_{1-x}Ti_x)_{23}$ (R=Nd, Tb).[33,34] For the Nd compound[33] the temperature of the anomaly is almost coincident with a sharp increase of the K_1 anisotropy constant, apparently in agreement with the interpretation given in Ref. 7. But in the Tb-based compound,[34] though both phenomena are present, they appear at different temperatures, which means they are clearly uncorrelated.

To study this type of non-SRT anomaly we have chosen both the pure and hydrogenated family of $R_2Fe_{14}B$ compounds. We have synthesized fresh compounds, measured their $\chi_{ac}(T)$ and applied heat treatments with varying annealing time and temperature (Sec. III). Moreover, we have developed a model (Sec. IV) that describes consistently the magnetic susceptibility and the MAE data in terms of a disaccommodation process. Finally, the applicability of this model to other rare earth–intermetallic compounds has been tested.

II. EXPERIMENTAL DETAILS

The $R_2Fe_{14}B$ ingots have been synthesized by melting the constituent elements in a hf induction oven under argon atmosphere (P=1.2 bar). Each as-cast ingot was first polished with abrasive paper, to eliminate any oxide from the surface, and then powdered in air, in an agate mortar, to about 10 μm grain size. The powdered samples were wrapped in tantalum foil, sealed in silica capsules, annealed in a temperature controlled furnace during a programmed time and then quenched in water. To obtain epoxy-bonded oriented powders, a 1 T magnetic field was applied to the epoxy powder mixture while it cured.

Samples with maximum hydrogen content were prepared from the ingots, in an autoclave (H_2 at 22.5 bar and 300 °C). The amount of hydrogen was determined by gravimetry. The intermediate $R_2Fe_{14}BH_x$ compounds were synthesized by reaction, at 300–350 °C, of nominal proportions to obtain the desired x value, of the pure and fully hydrogenated compounds. Epoxy-bonded oriented powders were prepared as above.

The crystallinity and homogeneity of the compounds was assessed by x-ray powder diffraction. The Debye-Scherrer technique, in the Bragg-Brentano geometry and with Fe $K_{\alpha 1}$ and Cu K_α radiations, was used. The microstructural configuration was observed on powders by scanning electron microscopy (SEM) (25 kV operating voltage) and the elemental composition was checked on polished samples by energy dispersive spectroscopy in the same apparatus.

The complex ac susceptibility, both the in phase, χ', and the out of phase component, χ'', was measured in an induction ac susceptometer,[35] from 4.2 K to room temperature (RT) in an exciting field amplitude (120 Hz, unless otherwise mentioned) of 1 Oe. The anisotropy of the anomaly has been studied measuring χ in the parallel ($\chi_\parallel$) and in the perpendicular ($\chi_\perp$) direction with respect to the alignment axis of the epoxy-bonded samples, i.e., with respect to their easy magnetization direction (EMD). The MAE was characterized measuring the variation of the initial permeability, $\mu=\mu_0(1+\chi)$, as a function of time after demagnetizing the sample with an ac external field, whose amplitude decreased linearly with time.[36]

III. EXPERIMENTAL RESULTS

A. Magnetic characterization with ac magnetic susceptibility

The ac susceptibility of $R_2Fe_{14}B$ compounds at low exciting field is due to reversible rotation of the magnetization and to DWM.[9,12,13] Since we are interested in the non-SRT anomaly, we have focused our study on the temperature range where the first contribution to the magnetization is nonanomalous. Therefore, we hope that any anomalous variation in susceptibility will be only due to DWM.

In this section we present some selected and illustrative examples of our measurements. In Fig. 1, we show, for epoxy-bonded oriented $Ho_2Fe_{14}B$ powders the thermal dependence of $\chi'_\parallel$ and $\chi''_\parallel$ measured at frequencies which cover three decades. Notice that the anomaly appears clearly both in $\chi'_\parallel(T)$, which shows a round and asymmetric anomaly at the thermal range 150 to 250 K, and in $\chi''_\parallel(T)$, which shows an anomaly wider and one order of magnitude lower than the one for $\chi'_\parallel(T)$. A slight frequency dependence is observed in the low temperature side of the anomaly and no dependence is detected in the high temperature side. Above 300 K both $\chi'_\parallel$ and $\chi''_\parallel$ sharply increase for low frequency excitation (1 Hz).

In Fig. 2(a), we show the $\chi'(T)$ measurements for nonoriented $Nd_2Fe_{14}B$ powders. Two anomalies are present: one peak around 135 K, which corresponds to the SRT exhibited by this compound,[37] and a shoulder about 240 K, the anomaly of present interest. Figures 2(b) and 2(c) show $\chi'_\parallel$ and $\chi'_\perp$ measured on an epoxy-bonded oriented powder sample. The SRT peak is enhanced in $\chi'_\perp$, as expected.[9,12,13]

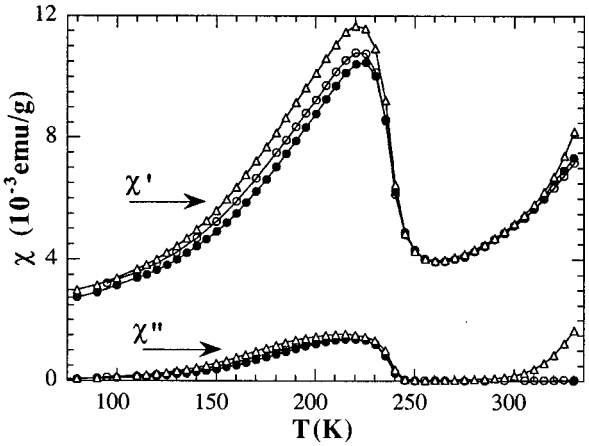

FIG. 1. In-phase, χ', and out-of-phase, χ'', magnetic susceptibility vs temperature of epoxy-bonded oriented $Ho_2Fe_{14}B$ powders measured along the EMD, at three different frequencies: △, 1 Hz; ○, 120 Hz; ●, 980 Hz.

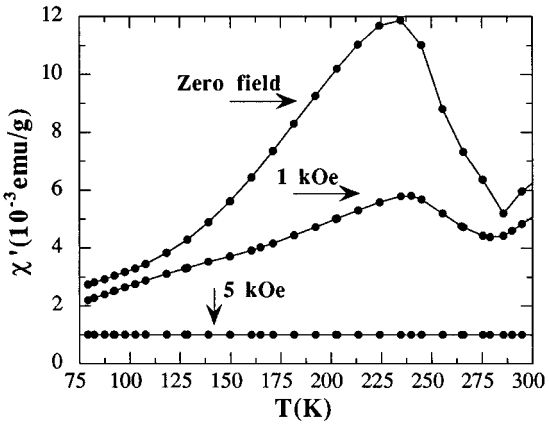

FIG. 3. $\chi'_{\parallel}$ vs temperature of epoxy-bonded oriented $Ho_2Fe_{14}B$ powders at different external dc fields, $H=0$, 1, and 5 kOe and applied parallel to the EMD.

In contrast, the anomaly near 240 K is enhanced in $\chi'_{\parallel}$, which implies a strong anisotropy. It has been observed that the grains of these materials are subdivided into 180° domains with their domain walls (DW) parallel to the c axis.[2–4] Since in the sample measured most grains have been aligned with their c axis parallel to the EMD, the mobility increase of these 180° DW give rise to an enhancement in $\chi'_{\parallel}$, while they give no contribution to $\chi'_{\perp}$, because DW are not moved by a small perpendicular exciting field.

In Fig. 3, we show $\chi'_{\parallel}(T)$ measured on epoxy-bonded oriented $Ho_2Fe_{14}B$ powders and with an external dc biasing magnetic field ($H=0$, 1, and 5 kOe) applied along the EMD direction. When the magnetic field increases the anomaly strongly reduces its height and disappears when the grains become single domains, at fields higher than 5 kOe as determined from hysteresis curves.

In Fig. 4(a), the presence of thermal hysteresis in the non-SRT anomaly for epoxy-bonded oriented $Ho_2Fe_{14}BH_{3.1}$ powders is demonstrated. In the cooling process the anomaly shifts to lower temperature with respect to its appearance in the warming run and its height strongly decreases. Another different thermal effect appears, namely that the height of the anomaly depends on the cooling rate that brings the sample to the starting temperature for a warming run [Fig. 4(b)]. As a conclusion, we can discern the non-SRT anomaly from the SRT one just studying the height enhancement in $\chi'_{\parallel}(T)$ and its thermal hysteresis.

The phenomenology involved in the non-SRT anomalies, and shared by all compounds which exhibit the anomaly, has been explored in a systematic study of the $R_2Fe_{14}BH_x$ series (R=Y, La, Ce, Pr, Nd, Sm, Gd, Tb, Dy, Ho, Er, Tm, Yb, Lu) and for x ranging from zero to the maximum hydrogen content. From this extensive set of measurements we have selected some of them to illustrate the common phenomenology.

(a) The anomaly is batch dependent. In Fig. 5 we show the measurements performed on $Ho_2Fe_{14}B$ stemming from two different batches. Both preparations were carried out un-

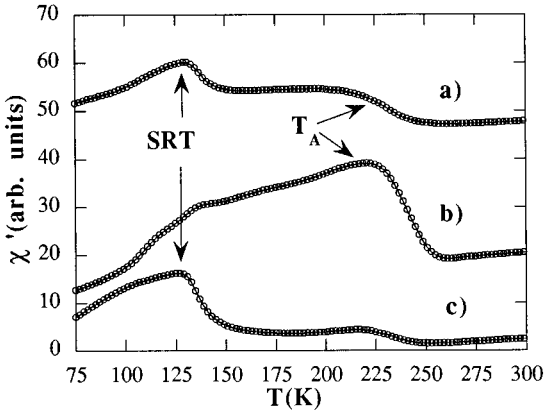

FIG. 2. χ' vs temperature for the $Nd_2Fe_{14}B$ compound, measured for different orientations: (a) free powder; (b) $\chi'_{\parallel}$, measured along the EMD in epoxy-bonded oriented powder; (c) $\chi'_{\perp}$, measured along the direction perpendicular to the EMD in epoxy-bonded oriented powder.

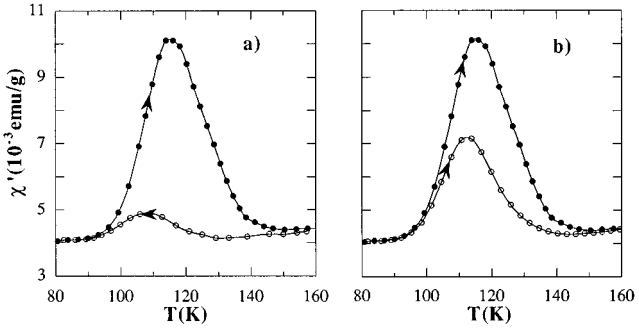

FIG. 4. $\chi'_{\parallel}$ vs temperature of epoxy-bonded oriented $Ho_2Fe_{14}BH_{3.1}$ powders at 120 Hz and under different thermal conditions: (a) measurements performed when heating (●) or cooling (○) the sample; (b) measurements performed heating the sample after a fast cooling (minutes) (●) of the sample, or a slow cooling (hours) (○).

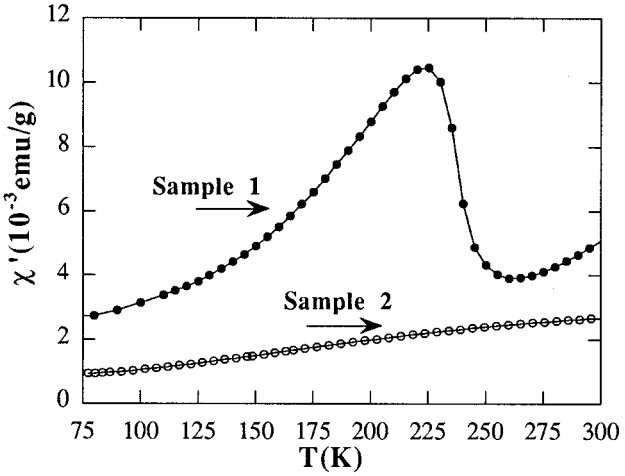

FIG. 5. χ' vs temperature of two samples of $Ho_2Fe_{14}B$ coming from different batches.

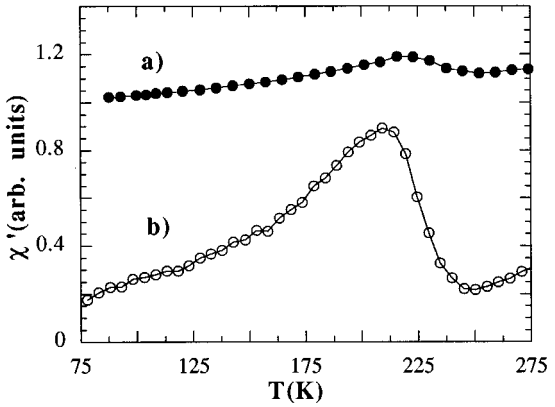

FIG. 7. χ' vs temperature of two samples of the compound $Dy_2Fe_{14}B$: (a) ingot sample; (b) free powder resulting form crushing the same ingot.

der as identical as possible conditions. The samples were checked by x-ray powder diffraction and they showed identical diffractograms. In one of the samples the anomaly clearly appeared at 240 K, but in the other one no anomaly was observed in the whole thermal range.

(b) In $R_2Fe_{14}B$ compounds the anomaly may appear for any R atom, even if R is nonmagnetic (R=Y, La, Lu). In Fig. 6 we show $\chi'_{\parallel}$ and $\chi''_{\parallel}$ for epoxy-bonded oriented $Y_2Fe_{14}B$ powders. The anomaly is clearly observed and presents its characteristic thermal hysteresis.

(c) The anomaly may appear irrespective of the crystal size of the sample. For example, it had been detected in a $Nd_2Fe_{14}B$ single crystal[9] and we have detected it in as-cast ingots, in free powder and in magnetically oriented powders.

(d) The relative size of the anomaly, once it appears, may depend on grain size. In Fig. 7(a) we show that for $Dy_2Fe_{14}B$ the as-cast ingot yields a lower maximum than the one for the crushed powder (10 μm grain size) [Fig. 7(b)].

(e) The anomaly temperature depends on hydrogen concentration. In Fig. 8(b), we show $\chi'_{\parallel}(T)$ for epoxy-bonded oriented $Ho_2Fe_{14}BH_x$ powders. The anomaly which the pure compound presents near 240 K is progressively shifted to lower temperatures, with increasing x, down to about 130 K (for $x \geq 2$). The same phenomenology occurs in other series (R=Ho, Tb, Pr, Nd, Y), as can be seen in Fig. 9, where we show the evolution of $T_A(x)$, the temperature at which there is an inflection point in $\chi'(T)$ above the maximum. All compounds have a similar dependence, but for the Y one, which has a less pronounced dependence.

B. Induction of the anomaly

To elucidate the origin of the anomaly we performed some physical and chemical modifications in the sample preparation procedure. We chose $Nd_2Fe_{14}B$ as test system, because for it the anomaly has clearly been observed[7,9] (see Fig. 2). Moreover, it also has a SRT (Ref. 37) in the appropriate thermal range (77 K to RT) and, therefore, the SRT anomaly may be used as a probe to determine how the pro-

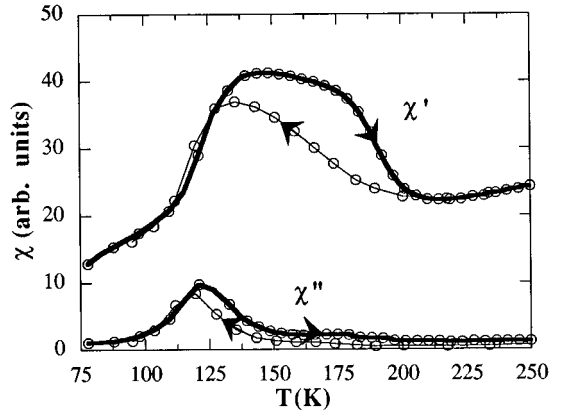

FIG. 6. $\chi'_{\parallel}$ and $\chi''_{\parallel}$ vs temperature of epoxy-bonded oriented $Y_2Fe_{14}B$ powders. Thick lines show the heating run, thin lines, the cooling run.

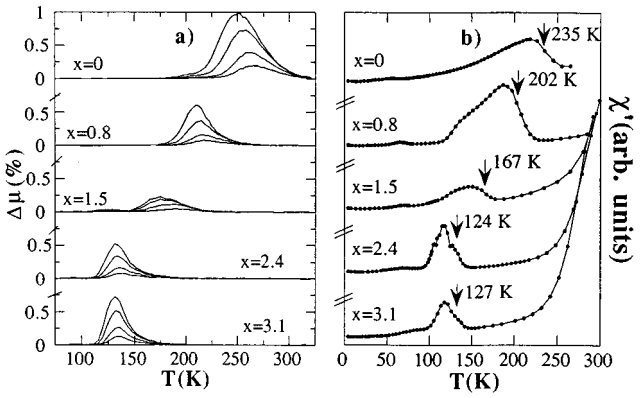

FIG. 8. (a) Isochronal relaxation curves performed on epoxy-bonded oriented $Ho_2Fe_{14}BH_x$ (x=0, 0.8, 1.5, 2.4, and 3.1) powders measured along the EMD, and for t_2=4, 8, 32, and 128 s. For each sample, the $\Delta\mu$ signal is higher for increasing t_2. (b) χ' vs temperature measurements performed over the same samples. The arrows mark the inflection point of the anomaly.

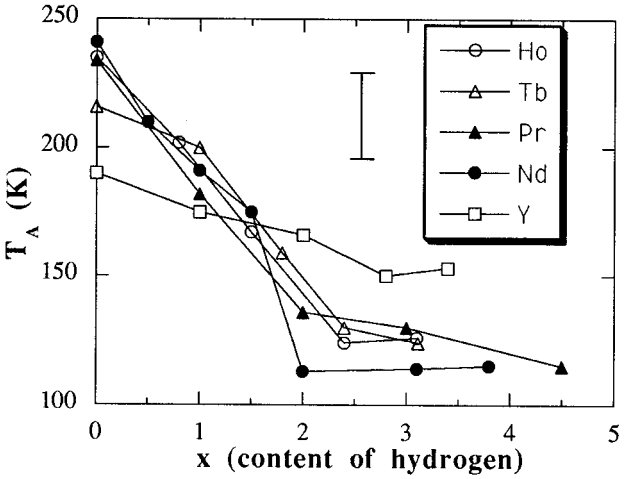

FIG. 9. Dependence of T_A with the hydrogen content in the $R_2Fe_{14}BH_x$ compounds (R=Ho, Tb, Pr, Nd, Y). The symbols indicate the minimum in $d\chi'/dT$ and the vertical bar represents the temperature range between the maximum value of $\chi'(T)$ in the anomaly and the minimum above the anomaly.

cessing affects this phase. For every testing step we have used different samples, which have always been taken from an unique batch. The effects on the induction of the anomaly, which the different modifications in the synthesis, annealing and subsequent quenching process produce on the compounds at room temperature, are summarized below.

(a) Nonstoichiometric compositions. Ingots with nominal composition Nd_2Fe_xB, x ranging from defect (x=11) to excess (x=15) with respect to the stoichiometric compound, were synthesized. From SEM measurements the existence of stoichiometric grains surrounded by Nd rich phase, other spurious phases, and α-Fe were clearly discernible for $x>14$. However, we could not correlate the existence of the anomaly with the presence of any secondary phases. Therefore, we conclude that neither the existence of other phases, nor the existence of α-Fe induces the anomaly.

(b) Surface oxidation. As-cast ingots, which had been in contact with air and humidity for years and had grown a thick oxide layer, showed no anomaly. On the other hand, an ingot which was well covered by a thick oxide layer and presented the anomaly, was polished and remeasured. The anomaly was not modified by the polishing process. We conclude that surface oxidation certainly does not induce or modify the anomaly.

(c) Annealing. The selected starting material was a stoichiometric sample which did not show any anomaly. The annealing process was performed after carefully sealing the sample in a silica capsule under pure argon atmosphere. After a given annealing time at each temperature the capsule was dipped in water to quench the compound to room temperature. To our surprise, the mere process of sealing the end of the capsule with a flame torch gave rise to the anomaly.

To clarify the effect of annealing we made some controlled experiments modifying two parameters: the annealing temperature and the annealing time. Moreover, to quantify the relative size of every anomaly we proceed as follows: The SRT is an intrinsic property and it is not affected by the

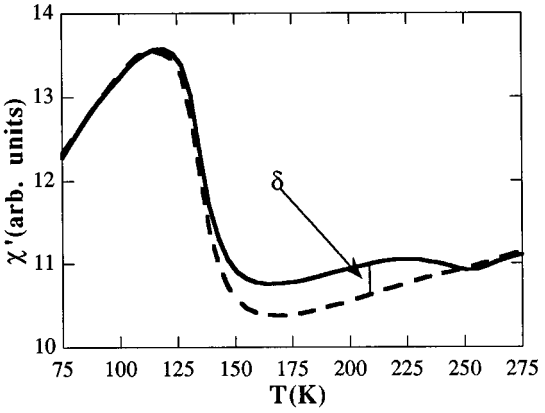

FIG. 10. χ' vs temperature of two $Nd_2Fe_{14}B$ free powders: one with the anomaly (continuous line) and another one without anomaly (dashed line). δ: see text.

annealing procedure. Therefore, for every thermally treated sample, χ' has been scaled to the non-anomalous χ', which we consider as the base line, just overlapping the SRT. The relative size of every anomaly has been quantified by $p(\%)=\delta/\chi'$, where δ is the difference between the value of χ' at the maximum of the anomaly and the value of χ' for the base line at the temperature of the maximum, and χ' is this last value (see Fig. 10). We have seen that p increases for any thermal treatment, either for fixed time and increasing annealing temperature (Fig. 11), or for fixed temperature and increasing annealing time.

To summarize this section we conclude the following: (a) in an as-cast ingot the anomaly appears only in some cases (depending on parameters out of our control such as the melting temperature, the melting time, the quenching process, etc.); (b) annealing and subsequent quenching always induces the anomaly, even if it was not present in the as-cast sample; (c) annealing and subsequent quenching enhances the anomaly, if previously present.

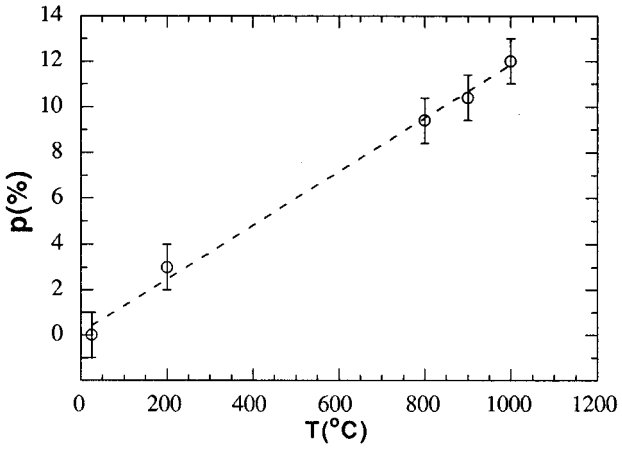

FIG. 11. Dependence of the relative size of the anomaly for $Nd_2Fe_{14}B$ powders (described by the parameter p; see text) with the annealing temperature, for an annealing time of three days.

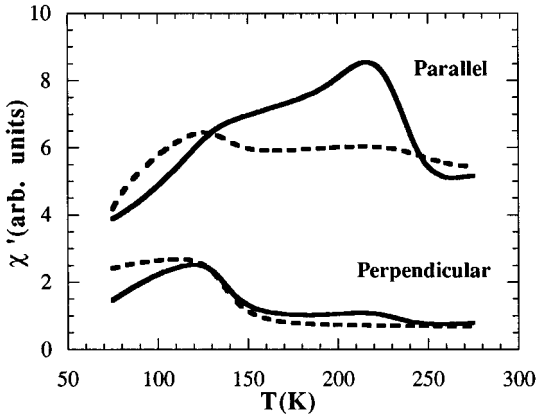

FIG. 12. $\chi'_{\parallel}$ and $\chi'_{\perp}$ vs temperature of two samples of epoxy-bonded oriented $Nd_2Fe_{14}B$ powders: (continuous line) sample with anomaly; (dashed lines) without anomaly.

C. Magnetic aftereffect measurements

The MAE measurements were performed on two epoxy-bonded oriented $Nd_2Fe_{14}B$ powders. The samples were from different batches; one of them had the non-SRT anomaly in $\chi_{ac}(T)$, while the other showed almost no anomaly (Fig. 12). We first applied a triangular demagnetization procedure and then measured, at each temperature, the variation of the initial magnetic permeability along the EMD, $\mu=\mu_0(1+\chi)$, as a function of time, between a fixed initial time t_1 and variable final time t_2. In Fig. 13 the $\Delta\mu(T)=\mu(T,t_1)-\mu(T,t_2)$ isochrones are shown, which correspond to the thermal dependence of the variation of the initial permeability between $t_1=2$ s and different $t_2=4$, 8, 32, and 128 s. There is a clear correspondence between the size of both anomalies; i.e., the larger the anomaly in $\chi'(T)$ is, the larger it is in MAE (continuous line in Figs. 12 and 13), on the contrary, when it is hardly present in $\chi'(T)$ it nearly disappears in MAE (dashed line in Figs. 12 and 13). Notice that in $Nd_2Fe_{14}B$ there is no MAE anomaly at $T_{SRT}=135$ K [Fig. 14(a)], which implies that in the time window of these experiments the magnetic moments are in equilibrium at the SRT temperature region.

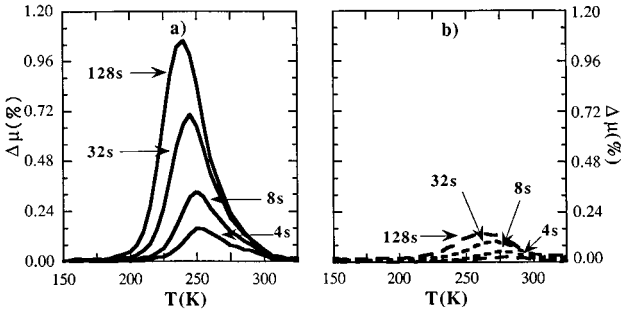

FIG. 13. Isochronal relaxation curves performed at different t_2 time on two samples of epoxy-bonded oriented $Nd_2Fe_{14}B$ powders: (a) corresponding to a sample that presents an anomaly in the susceptibility and (b) corresponding to a sample which presents no anomaly. MAE experiments were performed along the EMD. The samples used have been the same ones as those used in the measurements shown in Fig. 12.

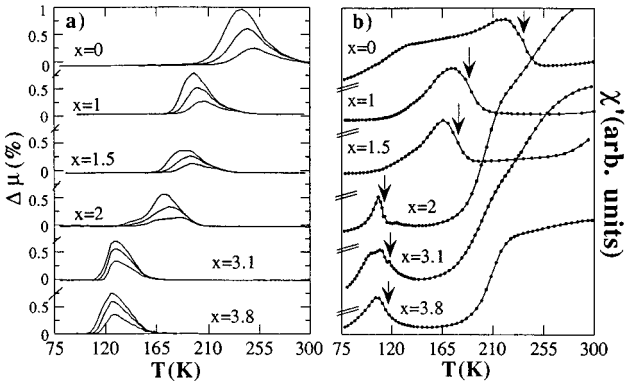

FIG. 14. (a) Isochronal relaxation curves performed on epoxy-bonded oriented $Nd_2Fe_{14}BH_x$ ($x=0$, 1, 1.5, 2, 3.1, and 3.8) powders measured along the EMD, and for $t_2=4$, 8, 32, and 128 s. For each sample, the $\Delta\mu$ anomaly is higher for increasing t_2. (b) χ' vs temperature measurements performed on the same samples. The arrows point to the inflection point of the anomaly.

We have also performed $\chi_{ac}(T)$ and MAE experiments on epoxy-bonded oriented $Nd_2Fe_{14}BH_x$ powders along the EMD. The correlation between the anomalies which appear in $\chi_{ac}(T)$ and MAE measurements is again evidenced (see Fig. 14); in both types of measurements the anomalies are shifted progressively to lower temperature for increasing x. As in the pure compound, the SRT of these compounds[38] do not give rise to a MAE anomaly.

In order to assure the correlation between $\chi_{ac}(T)$ and MAE for other R substitutions, we performed an analogous MAE study on the $Ho_2Fe_{14}BH_x$ compounds. Indeed, the thermal dependence of the MAE signal on these samples at different isochrones, Fig. 8(a), correlate with the χ' anomalies, Fig. 8(b), which proves the generality of this phenomenon.

At any rate, these experiments demonstrate clearly that there is a perfect correlation between the anomalies of both χ' and MAE for a given sample, so the underlying physical mechanisms which produce the anomalies, detected by two different experiments, must be the same.

IV. DISCUSSION

A. On the magnetic aftereffect

The above described experiments correspond to the reversible (or Richter type) MAE.[39] There are two microscopic mechanisms that can originate it: diffusion of defects in the crystal lattice, in a long-range process, or orientational after effects due to local reorientation of the symmetry axis of anisotropy defects, in a short-range process. Irrespective of the kind of process, the simplest modelization for the time-dependence of magnetic susceptibility corresponds to a Debye process, with a relaxation time τ, which follows the Arrhenius law,

$$\tau=\tau_0\ \exp(Q/k_BT), \tag{1}$$

where Q is the activation energy and k_B the Boltzman constant.

TABLE I. Activation energies, $\overline{Q}$, and inflection point, T_A, of the anomaly in χ' for different hydrogen concentrations. For both series of compounds the value $\overline{\tau_0}=(3\pm1)\times10^{-13}$ s has been obtained.

	$Ho_2Fe_{14}BH_x$			$Nd_2Fe_{14}BH_x$	
x (±0.1)	Q (eV) (±0.01 eV)	T_A (K) (±5 K)	x (±0.1)	Q (eV) (±0.01 eV)	T_A (K) (±5 K)
0.0	0.70	235	0.0	0.68	241
0.8	0.58	202	1.0	0.54	191
1.5	0.48	167	1.5	0.52	175
2.4	0.36	124	2.0	0.47	113
3.1	0.36	127	3.1	0.35	114
			3.8	0.34	114

The total interaction energy between the DW and the defects may be written as the sum of two contributions which are position dependent,

$$E_{\text{int}}(r)=E_1(r)+E_2(r). \tag{2}$$

$E_1(r)$ is a long-range term that results from the magnetostrictive interactions between the internal stresses of the defects and the elastic stresses of the DW. $E_2(r)$ is a short-range magnetocrystalline interaction which is attributed to local perturbations of the exchange interactions and the spin-orbit coupling energy.[40–43] The equilibrium distribution of DW and defects positions is determined by the minimum of this function.

In our MAE experiment an external field is applied, in a first step, which drives the magnetic system out of equilibrium. When, in a second step, the sample is subsequently demagnetized the DW's and defects are at off-equilibrium positions. Therefore the DW are not pinned to defects and χ' will be maximum since the mobility of DW's is also maximum. After demagnetization, the system will evolve towards equilibrium via the thermal activated process of defects moving towards minimum energy positions; this is called ''magnetic disaccommodation process.'' The motion of the defects to positions which allow for less mobility has the effect of reducing χ'.

The disaccommodation process originates a peak in the temperature dependent representation of $\Delta\chi(t_1,t_2,T)=\Delta\mu(t_1,t_2,T)$.[42] Though, in principle, there is a distribution of different relaxation times, we assume they may be averaged and that its expression may be described in terms of average prefactor time constant, $\overline{\tau_0}$, and average activation energy, $\overline{Q}$. The thermal and time decay of the susceptibility after demagnetization can be expressed as

$$\chi(t,T)=\chi_\infty(T)+\overline{\Delta\chi}\,\exp[-t/\tau(T)]. \tag{3}$$

We have fitted our MAE data (Figs. 8 and 14) on the $Nd_2Fe_{14}BH_x$ and $Ho_2Fe_{14}BH_x$ series, and have obtained an average value of $\overline{\tau_0}=(3\pm1)\times10^{-13}$ s, common for all compounds. In Table I we show $Q(x)$ together with the temperature, $T_A(x)$, at which the corresponding $\chi'(T)$ anomaly has an inflection point. When we compare $Q(x)$ for both series of compounds, we observe that they have very similar values for a given x. Also both $\overline{Q}(x)$ and $T_A(x)$ decrease rapidly for low values of x and tend towards constant values for $x\geqslant2$.

The MAE anomalies are consistently found about 250 K and their shape is rather sharp. By comparison to similar phenomenology in other compounds[43–46] we consider that short-range diffusion of vacancies or interstitial atoms is the most probable mechanism which modifies the DW mobility. We propose a two process model, similar to that proposed for the $Sm_2Fe_{17}H_x$ compounds,[25,26] to explain the anomaly; in the pure (or low hydrogen content) compounds the Fe vacancies are the most probable diffusing entities, while for higher x values the H atoms jump between different sites (though H atoms may be coupled to the Fe vacancies as well). In both cases the effect is a reorientation of the local anisotropy (orientational aftereffect). Indeed there are various reported examples of diffusion of Fe vacancies[47,48] or reorientation of H atoms[44,49] with similar values of $\overline{Q}(x)$, $\overline{\tau_0}$, and T_A.

We can describe the MAE phenomenology displayed in Sec. III in terms of the proposed model. In the pure compounds the anomaly appears on particular batches, only if sufficient vacancies are created and when their mobility is high enough. The annealing increases the density of vacancies and they are more homogeneously distributed and in the subsequent quenching process the new defects are blocked throughout the sample (in fact, this is a well documented procedure to create vacancies[50]). Since these point defects are coupled to the DW in the disaccommodation process, the higher the concentration and homogeneity of vacancies is, the more the DW become coupled to them. This has the effect of increasing $\overline{\Delta\chi}$ [Eq. (3)] without modifying $\overline{Q}$, which explains the increase of the height of the anomaly with increasing annealing temperature and time.

In the case of hydrogenated compounds, the existence of H-interstitial atoms ensures the existence of disaccommodation of the DW coupled to them. A simple thermodynamic model[49,51,52] may be adapted to explain the temperature dependence of the activation energy Q for H jumps between positions with discrete energy states. We recognize the fact that each site may be either occupied by just one H atom or remain empty. Therefore, a pseudo-Fermi Dirac statistical mechanics model may be applied to the H ensemble and, for a given H content, the chemical potential, μ, acts as a pseudo-Fermi level, which increases for increasing x. Consequently, μ corresponds to the energy of the H atom with

highest binding energy. In the equilibrium state μ increases as the interstitial sites are progressively filled for increasing x.

We may consider that the activation energy for the H jumps is

$$\overline{Q} = E_a - \mu, \tag{4}$$

where E_a is the average saddle point energy of the potential wells in which the H atoms are located and which have to be overcome in the diffusion process. If we assume that E_a is temperature independent, Q decreases as μ increases for increasing x. In fact, this is the tendency found experimentally.

As a conclusion, we propose that the relaxation process present in these systems is an orientational aftereffect of the local anisotropy due to the motion of Fe vacancies and H interstitial atoms.

B. On the ac magnetic susceptibility

Once we have shown in the previous section that the origin of the anomaly in MAE measurements is magnetic disaccommodation of DW coupled to point defects, we proceed to introduce the same model and parameters to interpret our $\chi_{ac}(T)$ data.

We may identify several characteristic time constants: τ, the average relaxation time of defects, given by the Arrhenius law; τ_m, the inverse of the excitation frequency and τ_e, the time span for every experimental point measurement. For our experimental conditions $\tau_m \approx 10^{-2}$ s and $\tau_e \approx 200$ s and are kept constant throughout the experiment, while τ decreases exponentially with increasing temperature [see Eq. (1)]. For $Nd_2Fe_{14}B$ and $Ho_2Fe_{14}B$ and with $\overline{\tau_0}$ and Q determined from MAE experiments we get for τ that it varies from 10^{30} s at 77 K to 10^{-3} s at 300 K. Therefore, to explain the global behavior of $\chi'(T)$ and $\chi''(T)$ the relative value of τ respect to τ_m and τ_e establishes four thermal ranges for increasing temperature, which are as follows.

(I) Metastable state range: $\tau \gg \tau_e \gg \tau_m$. DW's and defects are in non-thermodynamic equilibrium.

(II) Magnetic disaccommodation range: $\tau \approx \tau_e \gg \tau_m$. Defects and DW's reach the thermal equilibrium state in a disaccommodation process.

(III) Adiabatic regime: $\tau_e > \tau > \tau_m$. The system is in thermal equilibrium, but its response to the ac field is in the adiabatic regime; hence, defects cannot follow DW displacements at the excitation frequency.

(IV) Isothermal regime: $\tau_e \gg \tau_m \gg \tau$. The response to the ac field changes from the adiabatic regime to the isothermal one. Defects are able to follow the DW displacements at the excitation frequency.

To interpret the $\chi_{ac}(T)$ data we consider that in any of the four regimes there are two contributions: the background component, $\chi_0(T)$, and the contribution due to the presence of moving defects, $\chi_{md}(T)$, coupled to DW.

$\chi_0(T)$ is produced both by the reversible rotational process of the magnetic moments and by the motion of domain walls excited by the ac field. In the present work we simply determine it from the experiment on a sample without anomaly, and assume it to be additive to the contribution due to the presence of mobile defects coupled to DW.

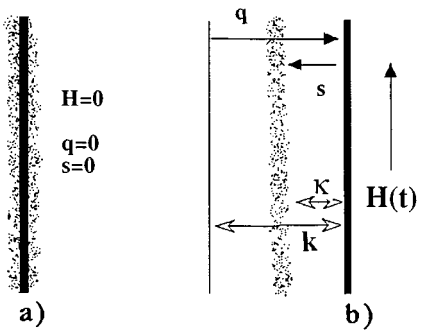

FIG. 15. Schematic representation of a domain wall coupled or pinned to point defects in two cases: (a) without external applied field; (b) with an external applied field parallel to the DW, that produces its movement. q and s represent the spatial coordinates; k and κ are the strength constants [see Eq. (5)].

The second component, $\chi_{md}(T)$, caused by the motion of the domain walls of a ferro(i)magnetic compound when excited by an alternating field in the presence of mobile defects, has been derived by Wantenaar *et al.*[53] In our χ_{ac} measurements the exciting magnetic field, $h = h_0 \sin \omega t$ exerts an alternating force on the DW, assumed to be pinned in a potential well with an intrinsic damping mechanism, therefore its equation of motion is that of a forced damped oscillator. The restoring force has two contributions: the first is associated with the intrinsic elastic coupling, that can be considered harmonic, the second corresponds to the attractive potential, which describes the interaction between walls and defects that act as pinning centers, as explained in Sec. IV A, Eq. (2). Besides, we have to consider that when a DW moves, the defects coupled to it will diffuse with an average relaxation time, τ. The equation that describes the whole motion is,

$$m\ddot{q} + \beta\dot{q} = -kq + \alpha H(t) + \kappa(r,s)s, \tag{5}$$

where m is the effective mass of the DW, q is the one-dimensional displacement of DW with respect to the equilibrium position at zero field (see Fig. 15), β is the damping coefficient which represents intrinsic wall losses, k is the elastic constant, α is the constant of proportionality linking the magnetic field $H(t)$ and the corresponding time dependent force on the wall, s is the instantaneous displacement from the DW (in the q direction) of the pinning center and $\kappa(r,s)$ represents an attractive potential between walls and pinning centers of range r. Since this potential is centered at the defects, hence it has a mobility defined by τ. Besides, we assume that the magnetization is proportional to the q displacements. In Fig. 15 we show schematically a DW and point defects acting as pinning centers. In the first case defects and DW are in equilibrium, whereas in the second case the DW moves under the excitation of the applied field and the defects try to follow this displacement.

Assuming an attractive harmonic potential of infinite range [so that $\kappa(r,s) = \text{constant}$, and scaling $\kappa = \kappa/k$], the equations that describe the dependence of χ' and χ'' (adimensional) with the external excitation frequency, $\nu = 2\pi\omega$, are

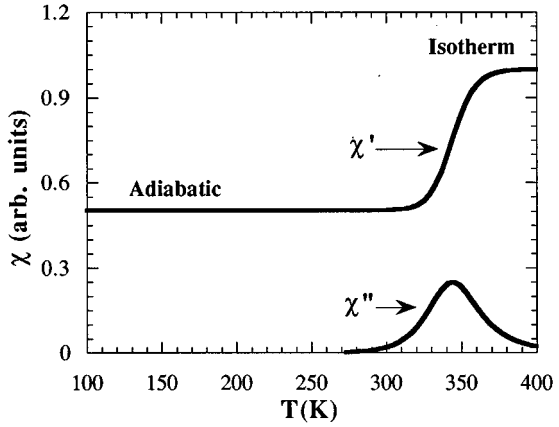

FIG. 16. Temperature dependence of χ'_{Deb} and χ''_{Deb} predicted by Eq. (7) for the $Ho_2Fe_{14}B$ compound.

$$\chi' = \frac{1+\omega^2\tau^2(1+\kappa)}{1+\omega^2\tau^2(1+\kappa)^2},$$

$$\chi'' = \frac{-\omega\tau\kappa}{1+\omega^2\tau^2(1+\kappa)^2}. \tag{6}$$

Though this is, in fact, a Debye-type relaxation process, in the present case τ is temperature dependent, while the frequency of the external ac field is kept constant. The temperature dependence of these functions can be obtained combining Eqs. (1) and (6),

$$\chi'_{\mathrm{Deb}}(T) = \chi'_{\mathrm{Deb}}(T=\infty)\,\frac{1+\omega^2(1+\kappa)\overline{\tau_0^2}\exp(2\overline{Q}/k_BT)}{1+\omega^2(1+\kappa)^2\overline{\tau_0^2}\exp(2\overline{Q}/k_BT)},$$

$$\chi''_{\mathrm{Deb}}(T) = \chi''_{\mathrm{Deb}}(T=\infty)\,\frac{-\omega\kappa\overline{\tau_0}\exp(\overline{Q}/k_BT)}{1+\omega^2(1+\kappa)^2\overline{\tau_0^2}\exp(2\overline{Q}/k_BT)}. \tag{7}$$

$\overline{Q}$ and $\overline{\tau_0}$ were determined for several compounds from MAE measurements, (see Table I) and the κ constant can be determined from appropriate experimental data, since $\chi'(T\to\infty)/\chi'(T=0)\approx 1+\kappa$. The resulting susceptibilities from Eq. (7) as a function of temperature are depicted in Fig. 16.

At low temperature, $\tau \gg \tau_m$, defects cannot follow the DW displacements because, within the time span of the ac exciting field period, their diffusion is too slow. The pinning centers (and potentials caused by them) remain superimposed on the intrinsical harmonic well potential. This superposition of static potentials reduces the magnitude of DW displacement and, therefore, there is a reduction of χ' to the so-called adiabatic susceptibility limit. Since there is no movement of defects, there is no time-delay in the response and consequently, no losses are observed in χ''. At high temperatures, $\tau \ll \tau_m$, when the thermally activated diffusion works, the defects respond fast to any DW displacement. Since the DW motion is accommodated at all times, the DW is not influenced by the pinning center and is effectively unpinned. Therefore χ' is higher and corresponds to the isothermal susceptibility. At intermediate temperatures, $\tau \approx \tau_m$, the DW speed is close to the rate of pinning centers diffusion. The appearance of a lag between DW and defect displacements gives rise to a maximum in $\chi''(T)$ at the temperature of the inflection point of $\chi'(T)$.

The magnetic disaccommodation process, which causes the MAE anomalies, produces a third type of contribution to the dynamic susceptibility. This fact may be explained if we analyze the methodology of the $\chi'(T)$ measurements and we take into account the values of the relaxation time, τ, compared to the measuring time of a point, τ_e, at different temperatures. Usually one starts cooling from RT, where τ is very low, and both defects and DW's are in equilibrium. When 77 K is reached the condition $\tau \gg \tau_e$ holds, and τ is so large that the system has not enough time to achieve its equilibrium state, after the time τ_e has elapsed; i.e., it is in a metastable state, the defects are fixed and the DW's move due to the ac field. Hence χ' will be higher than when the system is in equilibrium at that temperature, as we know from MAE experiments [see Eq. (3)]. When we start measuring a point we warm the sample and $\chi'(T)$ follows the background temperature dependence, since the system remains in a metastable state. As temperature increases, τ decreases exponentially and around 220 K the condition $\tau \approx \tau_e$ is achieved. Then the system starts the disaccommodation process towards equilibrium producing a decrease of χ'. We propose the time evolution equation,

$$\chi'_{\mathrm{dis}}(T,t) = \chi'_{\mathrm{dis}}\exp[-t/\overline{\tau_0}\exp(\overline{Q}/k_BT)] \tag{8}$$

as the simplest expression to describe this process; t corresponds to the time elapsed between the beginning of the heating process for a new point and the actual measuring time. It is, thus, the time of the transitory process while the system is in the metastable phase.

This process implies that in the disaccommodation regime there is a delay between the movements of the defects and of the DW's and, as a consequence there is an associated out of phase component in the susceptibility. The expression for this component is identical to Eq. (7), with ω substituted by its characteristic frequency, $\omega_e = \tau_e^{-1}$,

$$\chi'_{\mathrm{dis}}(T) = \chi''_{\mathrm{dis}}\,\frac{-\omega_e\kappa\overline{\tau_0}\exp(\overline{Q}/k_BT)}{1+\omega_e^2(1+\kappa)^2\overline{\tau_0^2}\exp(2\overline{Q}/k_BT)}. \tag{9}$$

The total complex susceptibility may then be calculated for each compound as

$$\chi(T) = \chi_0(T) + \chi_{\mathrm{Deb}}(T) + \chi_{\mathrm{dis}}(T). \tag{10}$$

Since χ_0, $\overline{\tau_0}$, and $\overline{Q}$ are known from appropriate experiments, we may then fit Eq. (10) to $\chi_{\mathrm{ac}}(T)$ experimental curves, where only $\chi_{\mathrm{Deb}}(T=\infty)$ and χ_{dis} are the fitting parameters.

We have applied this fitting procedure to the $Ho_2Fe_{14}B$ data because it has no other transition in the thermal range of interest that could also contribute to the experimental signal, and for this compound χ_0 can be experimentally determined

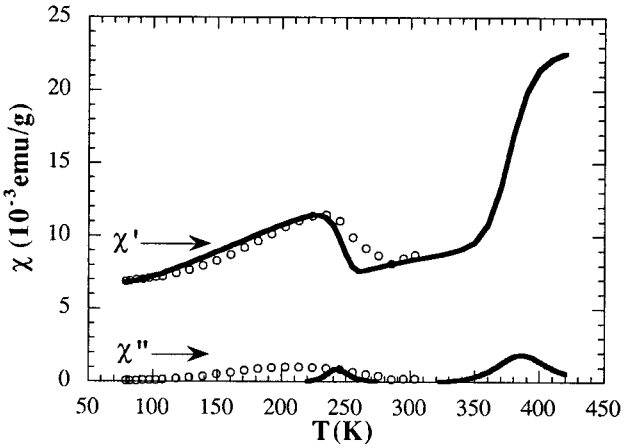

FIG. 17. Temperature dependence of χ' and χ'' of $Ho_2Fe_{14}B$. Both the experimental data (circles) and the theoretical curves obtained from Eq. (10) are shown.

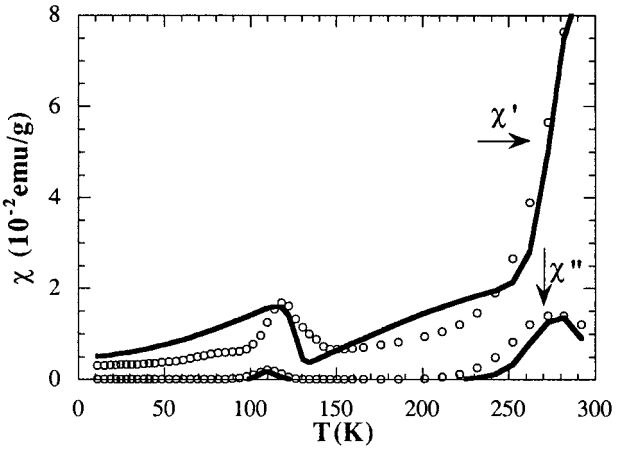

FIG. 18. Temperature dependence of χ' and χ'' of $Ho_2Fe_{14}BH_{3.1}$. Both the experimental data (circles) and the theoretical curves obtained from Eq. (10) are shown.

from a sample with no anomaly (Fig. 5). In Fig. 17 we compare the experimental data to the theoretical curve [Eq. (10)] calculated with fit parameters $\chi_{\mathrm{Deb}}(T=\infty)$ and χ_{dis} collected in Table II. The agreement between theory and experiment explains satisfactorily the existence of the anomaly at $T=235$ K, and its temperature dependence, as due to magnetic disaccommodation of DW's coupled to defects.

Though we observe the I, II, and III regimes, the steplike prediction corresponding to the existence of regime IV cannot be confirmed in this case, because it is out of the experimental thermal range. The experimental $\chi''(T)$ has a broad maximum centered at 220 K, while our prediction yields a sharper maximum centered at 245 K. This discrepancy is probably related to the simplifying assumption of just having one Q value, instead of a distribution of Q values.

Besides, Eq. (10) also predicts a second maximum in $\chi''(T)$ at higher temperatures, which cannot be confirmed clearly with this compound, although at lower frequencies it may be hinted (see Fig. 1). A possibility to confirm the predicted existence of a steplike anomaly in $\chi'(T)$ and the associated anomaly in $\chi''(T)$ is to perform the measurements on compounds with defect-jumps activation energy lower that in $Ho_2Fe_{14}B$. This can be easily achieved using hydrogenated compounds, since increasing x reduces Q (see Table I). Indeed, our data for $Ho_2Fe_{14}BH_{3.1}$ (Fig. 18) show the expected step at $T=270$ K. Taking the appropriate Q and $\overline{\tau_0}$ values, we have fitted the experimental curve in the four regimes and the parameters obtained are shown in Table II. We predict correctly the anomaly in $\chi'(T)$ at 100 K, though the experimental one is sharper. Moreover, the two experimental peaks in $\chi''(T)$ (Fig. 18) are reproduced in temperature by our theoretical prediction. However, the experimental peaks are again broader than the theoretical ones.

In order to observe clearly the transition from the adiabatic to the isothermal regime, i.e., the step in the $\chi'(T)$ component, we show in Fig. 19 the experimental data and the fit (with parameters shown in Table II) of the hydrogenated compound with the lowest Q: $Nd_2Fe_{14}BH_{3.8}$. In this compound the predicted step at high temperatures in the $\chi'(T)$ component and the two peaks in the $\chi''(T)$ component are nicely observed and fitted.

This agreement between theory and experiment can be confirmed using another family of compounds, which show the whole phenomenology here discussed. For example, the Sm_2Fe_{17} compound presents the anomaly in $\chi'(T)$ at around 150 K,[22,25] as determined from MAE measurements. In Fig. 20, we show the experimental $\chi'(T)$ for Sm_2Fe_{17}, together with the theoretical curve, Eq. (10), fitted with the parameters of Table II and Q and τ_0 taken from Ref. 25. Another example on which data are published is the $CeFe_2$ compound.[49] The $\chi'(T)$ data for $CeFe_2$ show the same behavior as Sm_2Fe_{17}. In Fig. 21, we show the experimental $\chi'(T)$ for $CeFe_2$, together with the theoretical curve, Eq. (10), fitted with the parameters of Table II and Q and $\overline{\tau_0}$

TABLE II. Parameters used in the theoretical fits performed with Eq. (10) and plotted in Figs. 17–21.

Compound	$\overline{Q}$ (eV)	$\overline{\tau_0}$ (s)	κ (adi.)	χ'_{Deb} $(T=\infty)$ (emu/g)	χ'_{dis} (emu/g)
$Ho_2Fe_{14}B$	0.70	3×10^{-13}	2.00	0.003	0.010
$Ho_2Fe_{14}BH_{3.1}$	0.36	3×10^{-13}	4.50	0.060	0.015
$Nd_2Fe_{14}BH_{3.8}$	0.34	3×10^{-13}	3.20	0.025	0.010
Sm_2Fe_{17}	0.51	1.8×10^{-13}	1.25	0.040	0.040
$CeFe_2$	0.20	1×10^{-14}	1.20	0.020	0.020

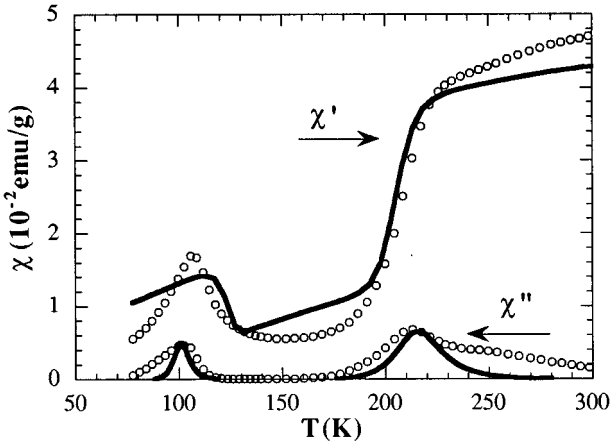

FIG. 19. Temperature dependence of χ' and χ'' of $Nd_2Fe_{14}BH_{3.8}$. Both the experimental data (circles) and the theoretical curves obtained from Eq. (10) are shown.

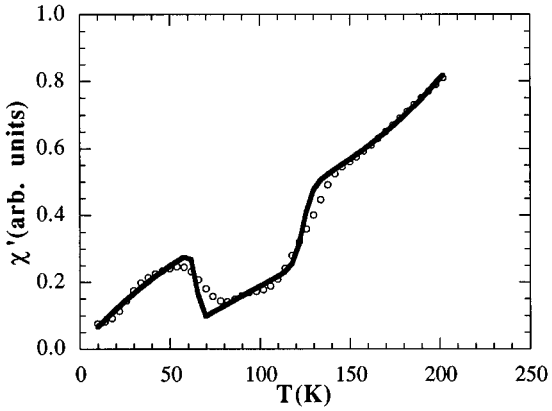

FIG. 21. Temperature dependence of the in-phase component of magnetic susceptibility for $CeFe_2$. Both the experimental data (circles) taken from Ref. 49, and theoretical curve obtained from Eq. (10) are shown.

taken from Ref. 49. In both cases the proposed model nicely fits the experimental data in the four regimes commented above. The same fit procedure may be applied to other reported anomalies in the $\chi'(T)$ for compounds with magnetic disaccommodation, like the $ZrFe_2$ Laves phase of Ref. 54. These results show that the applicability of our model is general to describe the behavior of the magnetic susceptibility in the presence of a magnetic disaccommodation process.

V. CONCLUDING REMARKS

The above proposed model, based on diffusion of Fe vacancies or H jumps and its influence on the mobility of DW's, have allowed us to explain the phenomenology reported in Sec. III. The model lies on the assumption that enough vacancies are produced by quenching of the melt, and that the defects are free to diffuse by thermal annealing. In the present work, our observation of induction of the anomaly by annealing, and its enhancement by increasing annealing time and temperature endorses these assumptions. At any rate, it is well known[50] that annealing and subsequent quenching process will lead to an increase of the density of vacancies of a crystalline solid at room temperature, and that the defects diffuse towards homogeneity by annealing.

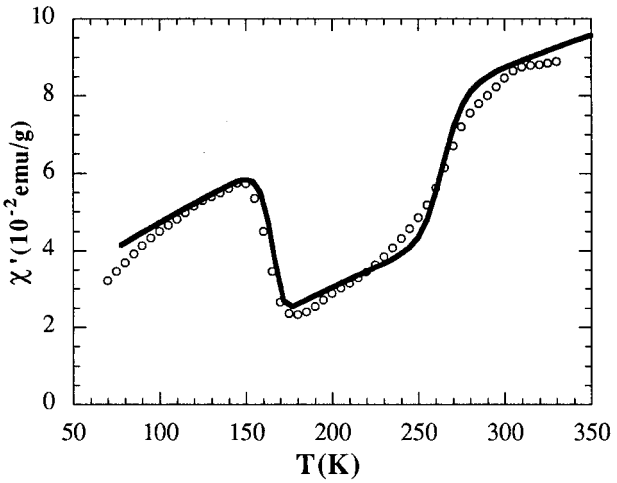

FIG. 20. Temperature dependence of the in-phase component of magnetic susceptibility for Sm_2Fe_{17}. Both the experimental data (circles) and the theoretical curve obtained from Eq. (10) are shown.

The main contribution to the magnetic susceptibility is given by the response of the DW parallel to the exciting field. Therefore, the anomaly appears mainly in the EMD, Fig. 2, and it is reduced in height under application of dc magnetic fields, Fig. 3. Since in thermal range I the system is out of the equilibrium, one expects thermal hysteresis in the anomaly, Fig. 4(a), and a strong dependence of $\chi'(T)$ with the cooling rate, Fig. 4(b).

The increase in the anomaly height, caused by crushing the polycrystalline ingot to powder (Fig. 7), may be related to the increase in DW's density, due to reduction of particle size. Indeed, when the size of a magnetic grain is reduced the domain width decreases with the square root of the grain thickness[55] causing the DW's density to increase, provided the grain size is above the threshold of single domain particles size (0.1 μm in these materials[56]).

The R atom plays no fundamental role in the model since the dominant interaction is the coupling of defects with DW's. This explains why the anomaly appears irrespective of R (Fig. 9). R may have influence on the activation energy, which reflects small differences in cell parameters and interatomic distances.

The reduction of the effective activation energy with increasing hydrogen content reflects the progressive filling and eventual saturation of the possible interstitial sites, where the hydrogen may be located, as explained in detail in Sec. IV A.

On the other hand, that the actual crystal structure modifies the activation energy is proven by the appearance of the anomaly at different temperatures for compounds belonging to different series, like the $R_2Fe_{17}H_x$ compounds.

In short, all common features that MAE, $\chi'(T)$ and $\chi''(T)$ experiments show, have been explained in terms of a phenomenological model of coupled defects and DW's, with their relaxation time dependent on temperature through an Arrhenius law.

ACKNOWLEDGMENTS

This work has been supported by the Spanish Project No. MAT 93-0240-C04-04 and CEAM III European project. We are indebted to F. Luis, C. Piquer, Professor D. Fruchart and Professor H. Kronmüller for the interesting and fruitful discussions as well as to Professor D. Gonzalez for a careful reading of the manuscript.

[1] R. A. Hein, in *Magnetic Susceptibility of Superconductors and Other Spin Systems*, edited by R. A. Hein *et al.* (Plenum, New York, 1991).

[2] K. H. J. Buschow, in *Ferromagnetic Materials*, edited by E. P. Wohlfarth and K. H. J. Buschow (Elsevier Science B.V., New York, 1988), Vol. 4, Chap. 1.

[3] K. H. J. Buschow, Rep. Prog. Phys. **54**, 1123 (1991).

[4] J. F. Herbst, Rev. Mod. Phys. **63**, 819 (1991).

[5] R. Grössinger, X. K. Sun, R. Eibler, K. H. J. Buschow, and H. R. Kirchmayr, J. Magn. Magn. Mater. **58**, 55 (1986).

[6] X. C. Kou, R. Grössinger, and H. R. Kirchmayr, J. Appl. Phys. **70**, 6372 (1991).

[7] X. C. Kou and R. Grössinger, J. Magn. Magn. Mater. **95**, 184 (1991).

[8] Z. G. Zhao, J. Y. Wang, Y. P. Ge, F. M. Yang, X. K. Sun, Y. C. Chuang, K. H. J. Buschow, and F. R. de Boer, J. Appl. Phys. **73**, 5875 (1993).

[9] D. X. Chen, V. Skumryev, and H. Kronmüller, Phys. Rev. B **46**, 3496 (1992).

[10] F. J. Lázaro, L. M. García, F. Luis, C. Rillo, J. Bartolomé, D. Fruchart, O. Isnard, S. Miraglia, S. Obbade, and K. H. J. Buschow, J. Magn. Magn. Mater. **101**, 372 (1991).

[11] F. J. Lázaro, L. M. García, J. Bartolomé, S. Miraglia, and D. Fruchart, in *Proceedings of the International Workshop on Studies of Magnetic Properties of Fine Particles*, edited by J. L. Dormann and D. Fiorani (North-Holland, Amsterdam, 1992), p. 423.

[12] C. Rillo, J. Chaboy, R. Navarro, J. Bartolomé, D. Fruchart, B. Chenevier, A. Yaouanc, M. Sagawa, and S. Hirosawa, J. Appl. Phys. **64**, 5534 (1988).

[13] M. D. Kuz'min, L. M. García, M. Artigas, and J. Bartolomé, Phys. Rev. B **54**, 4093 (1996).

[14] S. Obbade, S. Miraglia, P. Wolfers, J. L. Soubeyroux, D. Fruchart, F. Lera, C. Rillo, B. Malaman, and G. le Caer, J. Less-Common Met. **171**, 71 (1991).

[15] D. Fruchart, L. Pontonnier, F. Vaillant, J. Bartolomé, J. M. Fernandez, J. A. Puertolas, C. Rillo, J. R. Regnard, A. Yaouanc, R. Fruchart, and P. L'Heritier, IEEE Trans. Magn. **24**, 1641 (1988).

[16] P. C. M. Gubbens, Ph.D. thesis, Delft University, The Netherlands, 1977.

[17] X. C. Kou, Ph.D. thesis, Vienna Tech. University, Austria, 1991.

[18] S. Miraglia, J. L. Soubeyroux, C. Kolbeck, O. Isnard, D. Fruchart, and M. Guillot, J. Less-Common Met. **171**, 51 (1991).

[19] R. Grössinger, X. C. Kou, T. H. Jacobs, and K. H. J. Buschow, J. Appl. Phys. **69**, 5596 (1991).

[20] X. C. Kou, R. Grössinger, M. Katter, J. Wecker, L. Schultz, T. H. Jacobs, and K. H. J. Buschow, J. Appl. Phys. **70**, 2272 (1991).

[21] X. C. Kou, R. Grössinger, X. Li, J. P. Liu, F. R. de Boer, M. Katter, J. Wecker, L. Schultz, T. H. Jacobs, and K. H. J. Buschow, J. Appl. Phys. **70**, 6015 (1991).

[22] H. Kronmüller (private communication).

[23] J. Bartolomé, L. M. García, F. J. Lázaro, Y. Grincourt, L. G. de la Fuente, C. de Francisco, J. M. Muñoz, and D. Fruchart, IEEE Trans. Magn. **30**, 577 (1994).

[24] L. M. García, J. Bartolomé, F. J. Lázaro, C. de Francisco, J. M. Muñoz, and D. Fruchart, J. Magn. Magn. Mater. **140–144**, 1049 (1995).

[25] M. L. Sartorelli, I. Kleinschroth, and H. Kronmüller, J. Magn. Magn. Mater. **140–144**, 997 (1995).

[26] M. L. Sartorelli and H. Kronmüller (unpublished).

[27] X. C. Kou, T. S. Zhao, R. Grössinger, and F. R. de Boer, Phys. Rev. B **46**, 6225 (1992).

[28] X. C. Kou, T. S. Zhao, R. Grössinger, H. R. Kirchmayr, X. Li, and F. R. de Boer, Phys. Rev. B **47**, 3231 (1993).

[29] X. C. Kou, C. Christides, R. Grössinger, H. R. Kirchmayr, and A. Kostikas, J. Magn. Magn. Mater. **104–107**, 1341 (1992).

[30] C. Christides, A. Kostikas, G. Zouganelis, V. Psycharis, X. C. Kou, and R. Grössinger, Phys. Rev. B **47**, 11 220 (1993).

[31] C. Christides, A. Kostikas, X. C. Kou, R. Grössinger, and D. Niarchos, J. Phys. Condens. Matter **5**, 8611 (1993).

[32] E. Tomey, M. Bacmann, D. Fruchart, J. L. Soubeyroux, and D. Gignoux, J. Alloys Compd. **231**, 195 (1995).

[33] L. Morellón, L. Pareti, P. A. Algarabel, F. Albertini, and M. R. Ibarra, J. Phys. Condens. Matter **6**, L397 (1994).

[34] M. R. Ibarra, L. Morellon, J. Blasco, L. Pareti, P. A. Algarabel, J. García, F. Albertini, A. Paoluzi, and G. Turilli, J. Phys. Condens. Matter **6**, L717 (1994).

[35] C. Rillo, F. Lera, A. Badía, L. A. Angurel, J. Bartolomé, F. Palacio, R. Navarro, and A. J. van Duyneveldt, in *Magnetic Susceptibility of Superconductors and Other Spin Systems*, edited by R. A. Hein (Plenum, New York, 1991).

[36] C. de Francisco, J. I. Iñiguez, J. M. Muñoz, and J. Ayala, IEEE Trans. Magn. **23**, 1866 (1987).

[37] D. Givord, H. S. Li, and R. P. de la Bathie, Solid State Commun. **51**, 857 (1984).

[38] M. D. Kuz'min, L. M. García, I. Plaza, J. Bartolomé, D. Fruchart, and K. H. J. Buschow, J. Magn. Magn. Mater. **146**, 77 (1995).

[39] B. D. Cullity, *Introduction to Magnetic Materials* (Addison-Wesley, Reading, MA, 1972).

[40] L. Néel, J. Phys. Rad. **12**, 339 (1951).

[41] L. Néel, J. Phys. Rad. **13**, 249 (1952).

[42] H. Kronmüller, *Nachwirkung in Ferromagnetika*, Springer Tracts in Natural Philosophy Vol. 12 (Springer, Berlin, 1968).

[43] B. Hohler and H. Kronmüller, J. Magn. Magn. Mater. **19**, 267 (1980).

[44] H. Kronmüller, in *Hydrogen in Metals I*, edited by G. Alefeld and J. Völkl (Springer, Berlin, 1978), Chap. 19.

[45] A. Hofmann and H. Kronmüller, Phys. Status Solidi A **104**, 381 (1987).

[46] M. Hirscher, in *Interstitial Intermetallic Alloys*, Vol. 281 of *NATO Advanced Study Institute, Series E: Applied Sciences*, edited by F. Grandjean, G. J. Long, and K. H. J. Buschow (Kluwer Academic, The Netherlands, 1995), p. 333.

[47] C. de Francisco, J. M. Muñoz, J. Ayala, and J. I. Iñiguez, Phys. Status Solidi A **108**, 721 (1988).

[48] C. de Francisco, R. Torres, J. M. Muñoz, and J. Rivas, Phys. Status Solidi A **123**, 297 (1991).
[49] E. H. Büchler, M. Hirscher, and H. Kronmüller, in *Interstitial Intermetallic Alloys* (Ref. 46), p. 521.
[50] F. Agulló-López, C. R. A. Catlow, and P. D. Townsend, *Point Defects in Materials* (Academic, New York, 1988), Chap. 7.
[51] R. Kirchheim, Acta Metall. **30**, 1069 (1982).
[52] R. Kirchheim, Prog. Mater. Sci. **32**, 262 (1988).
[53] G. H. T. Wantenaar, G. V. H. Wilson, D. H. Chaplin, and S. J. Campbell, J. Magn. Magn. Mater. **89**, 13 (1990).
[54] C. U. Maier and H. Kronmüller, J. Phys. Condens. Matter **4**, 4409 (1992).
[55] R. S. Wadas, *Magnetism in Spinels, Garnets and Perovskites* (Polish Academy of Sciences, Warszawa, 1974).
[56] H. Kronmüller, in *Supermagnets, Hard Magnetic Materials*, Vol. 331 of *NATO Advanced Study Institute, Series C: Mathematical and Physical Sciences*, edited by G. J. Long and F. Grandjean (Kluwer Academic, The Netherlands, 1990), Chap. 11.